Cell, Vol. 120, 343–355, February 11, 2005, Copyright ©2005 by Elsevier Inc. DOI 10.1016/j.cell.2005.01.024

Structural Analyses Reveal Phosphatidyl Inositols as Ligands for the NR5 Orphan Receptors SF-1 and LRH-1

Irina N. Krylova,[1,7] Elena P. Sablin,[2,7] Jamie Moore,[3] Robert X. Xu,[5] Gregory M. Waitt,[5] J. Andrew MacKay,[4] Dalia Juzumiene,[5] Jane M. Bynum,[5] Kevin Madauss,[5] Valerie Montana,[5] Lioudmila Lebedeva,[1] Miyuki Suzawa,[1] Jon D. Williams,[5] Shawn P. Williams,[5] Rodney K. Guy,[3] Joseph W. Thornton,[6] Robert J. Fletterick,[2] Timothy M. Willson,[5] and Holly A. Ingraham[1,*]

[1]Department of Physiology
[2]Department of Biochemistry and Biophysics
[3]Department of Pharmaceutical Chemistry
[4]Graduate Group in Bioengineering
1550 4th Street
Mission Bay Campus
University of California
San Francisco, California 94143
[5]Discovery Research
GlaxoSmithKline
5 Moore Drive
Research Triangle Park, North Carolina 27709
[6]Center for Ecology and Evolutionary Biology
321 Pacific Hall
University of Oregon
Eugene, Oregon 97403

Summary

Vertebrate members of the nuclear receptor NR5A subfamily, which includes steroidogenic factor 1 (SF-1) and liver receptor homolog 1 (LRH-1), regulate crucial aspects of development, endocrine homeostasis, and metabolism. Mouse LRH-1 is believed to be a ligand-independent transcription factor with a large and empty hydrophobic pocket. Here we present structural and biochemical data for three other NR5A members—mouse and human SF-1 and human LRH-1—which reveal that these receptors bind phosphatidyl inositol second messengers and that ligand binding is required for maximal activity. Evolutionary analysis of structure-function relationships across the SF-1/LRH-1 subfamily indicates that ligand binding is the ancestral state of NR5A receptors and was uniquely diminished or altered in the rodent LRH-1 lineage. We propose that phospholipids regulate gene expression by directly binding to NR5A nuclear receptors.

Introduction

Unlike most nuclear receptors, which are regulated by steroid, retinoid, and other nonpolar ligands, NR subfamily 5A are constitutively active in many cell types, and obvious ligand candidates have not been forthcoming. SF-1 (NR5A1) orchestrates endocrine tissue development and male sexual differentiation and controls steroid biosynthesis (Ingraham et al., 1994; Luo et al., 1994). LRH-1 (NR5A2) is essential in early development and regulates bile acid synthesis, cholesterol transport, and ovarian function (Fayard et al., 2004; Lu et al., 2000). This subfamily is distinct in that members are able to bind as monomers to DNA, and they possess an unusually large hinge domain that is subject to posttranslational modifications, including phosphorylation and sumoylation (Desclozeaux et al., 2002; Lee et al., 2005). Although physiological roles for these receptors have emerged, ligand candidates have remained controversial. The proposed SF-1 ligand 25-hydroxycholesterol, while appealing because of the receptor's regulation of steroid synthesis, appears to be incorrect because oxysterols fail to activate SF-1 in most cell lines (Christenson et al., 1998; Lala et al., 1997; Mellon and Bair, 1998). Further, the notion that ligands might be dispensable for this subfamily of receptors was bolstered by the crystal structure of mouse LRH-1 ligand binding domain (LBD), showing an active conformation in the absence of either ligand or coregulator peptide. Unlike other orphan nuclear receptors, which either lack a ligand binding pocket (e.g., Nurr1, DHR38, or ERRα) or have a constitutively bound lipid (e.g., HNF4α, HNF4γ, or USP), mLRH-1 was found to possess a large unoccupied hydrophobic pocket of ~830 Å (reviewed in Li et al. [2003]). Remarkably, mutations that filled the mLRH-1 pocket failed to reduce transcriptional activity (Sablin et al., 2003).

Whereas an elegant structural paradigm has developed to explain the activation of ligand-regulated receptors, no uniform mechanism has been proposed to account for the modulation of orphan nuclear receptor activity (Steinmetz et al., 2001; Weatherman et al., 1999). The presence of fortuitous lipid molecules revealed in crystallization experiments can be associated with an inactive LBD conformation as noted for the *dipterian* USP LBD (Billas et al., 2001). On the other hand, lipid components have been proposed to stabilize an active LBD conformation in constitutively active nuclear receptors, with HNF4 binding fatty acids (Dhe-Paganon et al., 2002; Wisely et al., 2002) and RORα binding cholesterol (Kallen et al., 2002). In this context, the structure of the murine LRH-1 with its empty ligand binding pocket remains a puzzle. To further explore how NR5A orphan receptors are regulated, we obtained the LBD crystal structures of other members of this subfamily, including mSF-1, hSF-1, and hLRH-1. Here we provide structural and biochemical data supporting ligand regulation for NR5A orphan nuclear receptors.

Results and Discussion

NR5A Structures Reveal a Phospholipid in the Ligand Binding Pocket

The structure of mSF-1 was determined by the molecular replacement method using the atomic coordinates from Protein Data Bank entry 1PK5 for the mLRH-1 LBD coordinates (Sablin et al., 2003). Two hSF-1 structures

*Correspondence: hollyi@itsa.ucsf.edu
[7]These authors contributed equally to this work.

Table 1. Data Collection and Refinement Statistics

Crystallization	mSF-1/mSHP-1	hSF-1/No Pep.	hSF-1/TIF-2	hLRH-1/TIF-2
Unit Cell Dimensions				
a (Å)	73.9	128.4	73.1	59.9
b (Å)	73.9	66.0	73.1	67.2
c (Å)	117.0	141.0	139.4	79.6
Space group	$P4_12_12$	$P2_1$	$P4_12_12$	$P2_12_12_1$
Molecules per asymmetric unit	1	7	1	1
Resolution (Å)	25–1.2	20–2.5	20–2.9	40–2.5
Number of unique reflections	100,431	71,698	15,614	10,787
Data redundancy	13.1	2	8	6
Completeness (%)	99.9	97.9	99.8	91.9
Rsymm (%)	6.1	4.5	5.8	3.7
< I/s(I) >	39.2	28.0	30.0	44.0
Refinement				
R	19.7	24.9	24.6	23.2
Rfree	21.1	28.3	29.0	28.3
Rms deviation from ideality				
Bond length (Å)	0.012	0.009	0.011	0.008
Bond angle (0)	1.483	1.20	1.34	1.349
Average B factor (A2)				
All atoms	22.8	85	62	64.4
Protein atoms	21.3	85	61	63.9
Water molecules	25.7	78	55	60.5

were obtained, with and without TIF-2 peptide, and were determined by MAD and SAD methods using selenomethionine substituted proteins, respectively (Madauss et al., 2004). The structure of hLRH-1 was determined by molecular replacement using the atomic coordinates for hSF-1. The current best structures are refined to 1.2 Å, 2.5 Å, and 2.5 Å for mSF-1, hLRH-1, and hSF-1, respectively. Relevant features of data collection and refinement statistics for each protein crystal are provided in Table 1. All three LBDs exhibit a characteristic protein fold noted for other LBDs, with 12 α helices, two β strands, and helix H12 positioned in an active conformation (Figure 1). A fourth layer is provided by a structured helix H2, as previously shown for mLRH-1, although the position and length of this helix are the most varied features as judged by comparison of mSF-1 with hSF-1 LBD (Figure 1C) and mLRH-1 with hLRH-1 (Figure 1D). Upon refinement of these three LBD structures, additional electron density was present in the ligand binding pockets consistent with the presence of a phospholipid; the presence of ligand contrasts the reported structure of mLRH-1 showing no density inside or at the opening of the pocket.

The nature of this phospholipid was further characterized by nondenaturing mass spectrometry of LBD proteins used for crystallization. Spectra were consistent with two principle series of ions consisting of both ligand bound and apo-proteins. Comparison of all four LBD protein solutions showed the presence of phospholipid in SF-1 and hLRH-1 but with a much lower concentration in mLRH-1 where only ~10% is bound by ligand (Figures 2A and 2B and Supplemental Figure S1 available with this article online). Quantitation of hLRH-1 and mSF-1 bound by phospholipid showed a 1:1 ligand/receptor complex with nearly all of the protein bound by a phospholipid. The lower levels of phospholipid bound to bacterially expressed mLRH-1 LBD are consistent with the absence of electron density in the pocket of the mLRH-1 LBD structure. Of possible ligands ranging from 680–780 Da, the most prominent species were found to be 747 and 721 Da, consistent with two common bacterial phospholipids, phosphatidyl glycerol (PG) and phosphatidyl ethanolamine (PE). Denaturing negative electrospray ionization assigned the prominent ligand species as PG (Figure 2C); confirmation of this assignment was provided by the atomic crystal structure of mSF-1, where the head group of the phospholipid was determined to be glycerol rather than ethanolamine (Figure 2D). Mutating Ala270 to Trp in helix H3 of mSF-1, which would fill the pocket and disfavor ligand binding, eliminates all detectable PG ligand from the pocket by mass spectrometry (A270W, Figure 2B).

Electron densities maps of mSF-1 or hSF-1 (± TIF peptide) showed nearly identical conformation of a phospholipid containing two fatty acid chains (C16 and C18) occupying nearly the entire hydrophobic pocket; only hydrophobic interactions are observed between the C16 and C18 chains and surrounding residues (Figures 2D, 2E, and Supplemental Table S1). Atomic resolution structure of mSF-1 LBD confirmed the presence of double bonds at the C9 position in both chains within the bound phospholipid. The large pocket sizes of hSF-1 and hLRH-1 are similar to that reported for the mLRH-1 LBD, easily accommodating two tails of the phospholipid. In hLRH-1, the ligand adopts a similar conformation or path as found for SF-1; however, the density is less ordered and the lower resolution prevented absolute assignment of the head group (data not shown). Nonetheless, we find that all phosphates are positioned similarly in the mouth of the pocket for mSF-1, hSF-1, and hLRH-1. Although a phospholipid ligand is present in both USP and NR5A, the consequences of ligand binding differ greatly, with ligand proposed to drive USP into an antagonist conformation, rather than the agonist state observed for NR5A receptors (Billas et al., 2001).

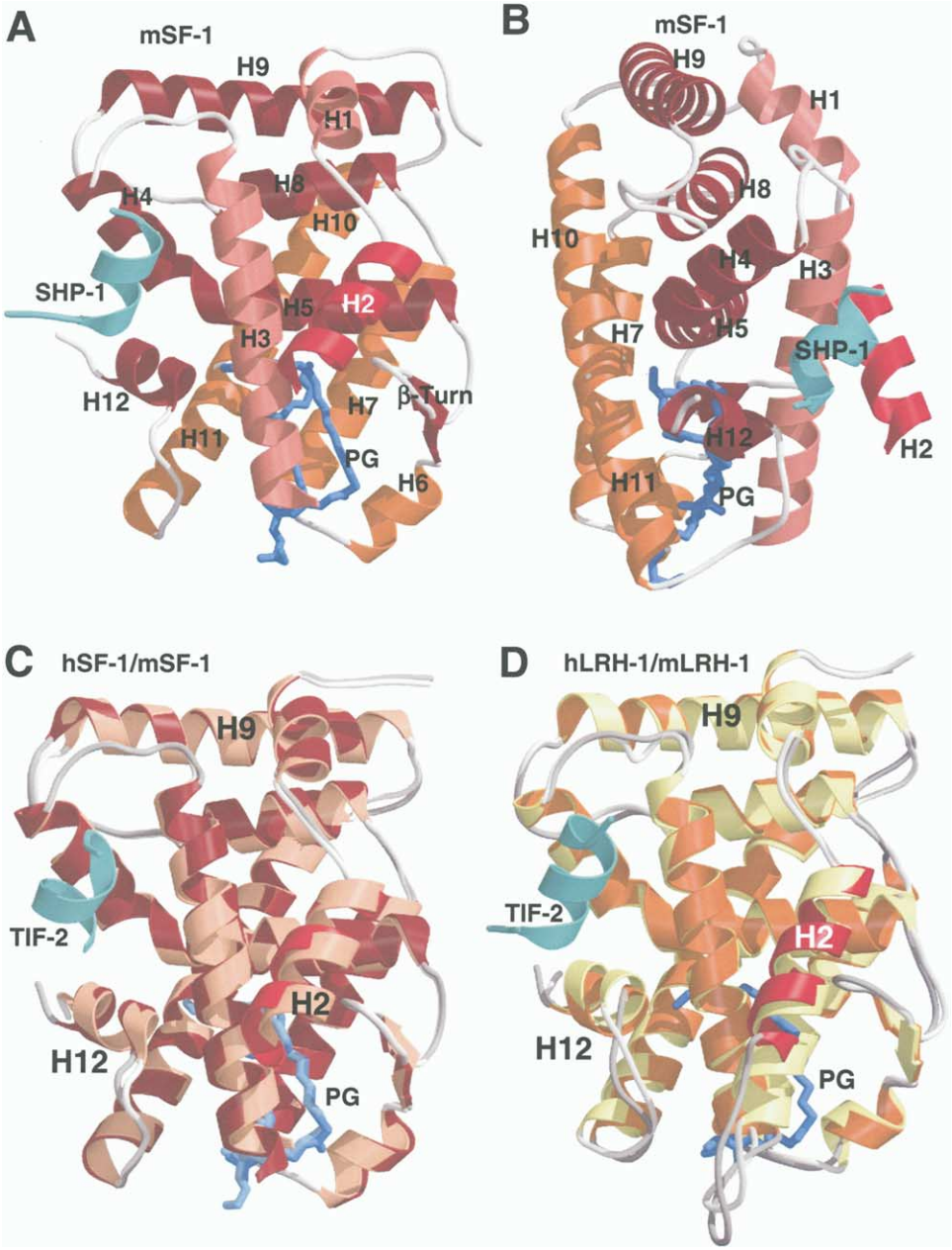

Figure 1. NR5A LBD Receptors Structures Reveal a Ligand

(A and B) Two views of mouse SF-1 (mSF-1) LBD protein are shown (red, orange, and brown ribbons) with all twelve α helices and the single β turn indicated in panels. Helix H2 is highlighted in bright red (H2). The corepressor peptide form the N-terminal portion of mSHP is shown in the AF2 cleft just adjacent to helix H12 (SHP-1, turquoise ribbon). The presence of a ligand determined to be phosphatidyl glycerol (PG) is also shown in the hydrophobic pocket (blue stick).

(C) The model for human SF-1 (hSF-1, dark red ribbons) superposed with the mSF-1 (light red) is shown.

(D) The human LRH-1 LBD (hLRH-1, orange ribbons) superposed with the mouse LRH-1 LBD (yellow ribbons) structure is shown. Helices H2, H9, and H12 are indicated in both structures, with H2 highlighted in red for all LBDs. For both hSF-1 and hLRH-1, the TIF-2 peptide bound structures are shown (refer to Table 1), and the phospholipid is indicated (PG, blue stick).

Phosphatidyl Inositol Phosphates Are Selectively Bound by SF-1 and hLRH-1

While our structural studies indicate that bacterially expressed SF-1 and LRH-1 can bind to phospholipids, the nature of a bona fide ligand in eukaryotic cells remains unknown. We tested the ability of mSF-1 to bind eukaryotic phospholipids, including phosphatidyl inositols (PIs), using immobilized lipids on nitrocellulose, as described in Experimental Procedures. Of the common eukaryotic phospholipids, mSF-1 and hLRH-1 selectively bound the PIP_2 and PIP_3 phosphatidyl inositol species 2- to 3-fold better than the pocket mutant pro-

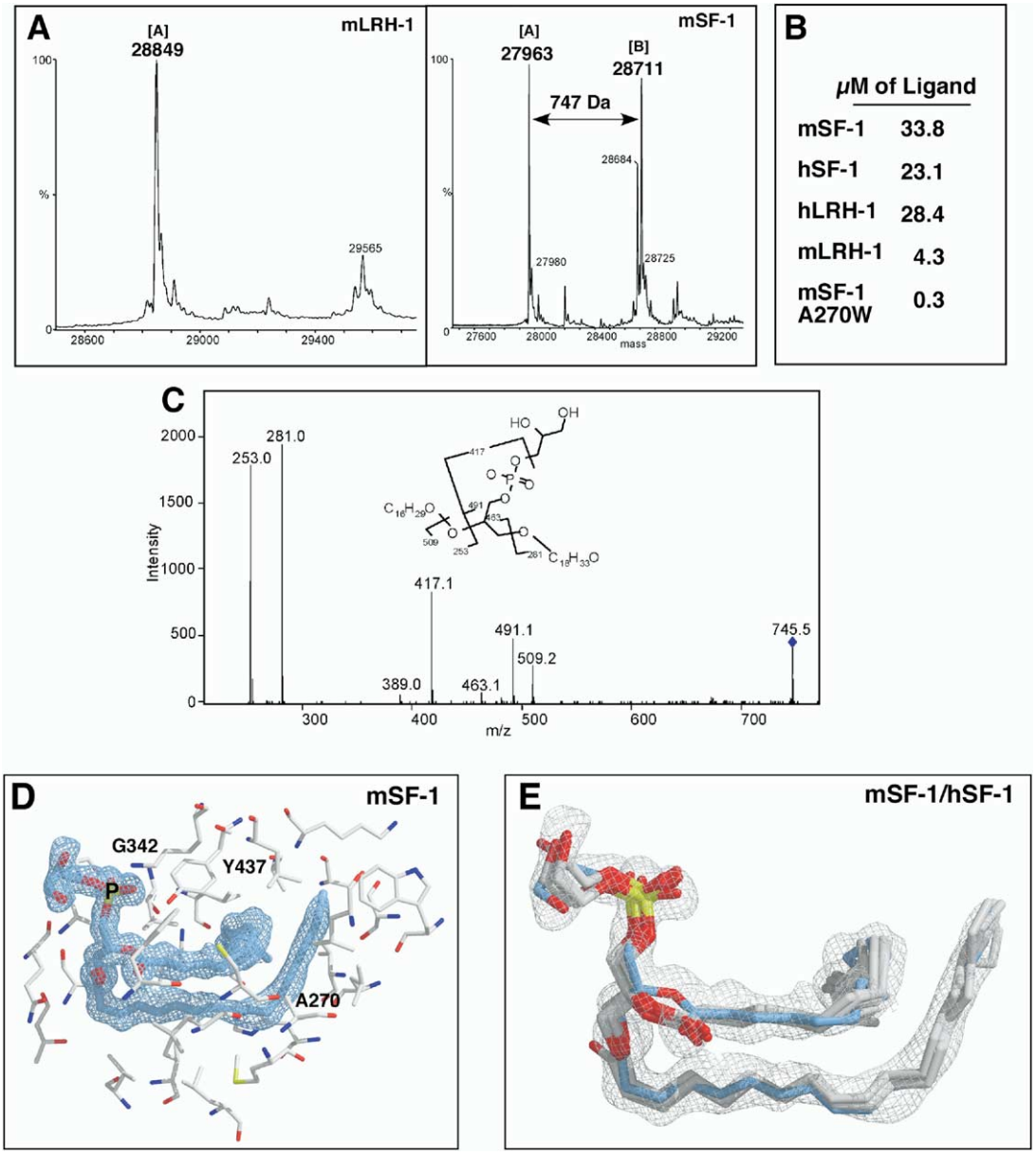

Figure 2. Binding of Phospholipids by SF-1s and hLRH-1 Is Greater than for mLRH-1 or for the mSF-1 A270W Pocket Mutant

(A) Nondenaturing mass spectrometry was carried out on all four LBD proteins used for crystallization (mSF-1, hSF-1 and mLRH-1, hLRH-1). Spectra are shown for mLRH-1 (left panel) and mSF-1 (right panel), with the apo [A], and the bound [B] species indicated. The molecular weight difference between the two peaks is also shown (arrow).

(B) The concentrations of all bound LBD species, including the mSF-1 A270W pocket mutant, were determined as described and are listed for equal amounts of LBD protein (~30 μM), with the exception of hSF-1, where more protein was used due to the poorer quality of protein (50 μM).

(C) Product ions following collision-induced decomposition using denaturing electrospray tandem mass spectrometry (ESI MS/MS) on m/z 745 (blue diamond) are shown for hSF-1 and reveal a phosphatidyl glycerol (chemical structure) ligand with two acyl chains of C16 and C18.

(D) Electron density for mSF-1 is from a 2Fo–Fc map contoured at 1.2 sigma that shows the phospholipid ligand flanked by surrounding residues (sticks). Three residues are labeled: Gly342, Tyr437, and Ala270, and the phosphate in the PG ligand is indicated (P).

(E) Electron density found for both mSF-1 (blue) and hSF-1 ± TIF peptide (white or gray) ligands are superposed showing an identical position in the hydrophobic ligand binding pocket.

tein (A270W, Figure 3A), with signals being especially strong for both PI(3,5)P_2 and PI(3,4,5)P_3. Both wild-type and mutant mSF-1 protein bound equally to PA or the single phosphorylated PIPs, suggesting that these negatively charged lipids bound to the solvent-exposed surface of the LBD. More importantly, equal amounts of incubated apo human PPARγ-LBD displayed much weaker binding with a different profile (Figure 3A, right panel), and no binding was detected with liganded hTRβ LBD (data not shown). The capacity to bind such

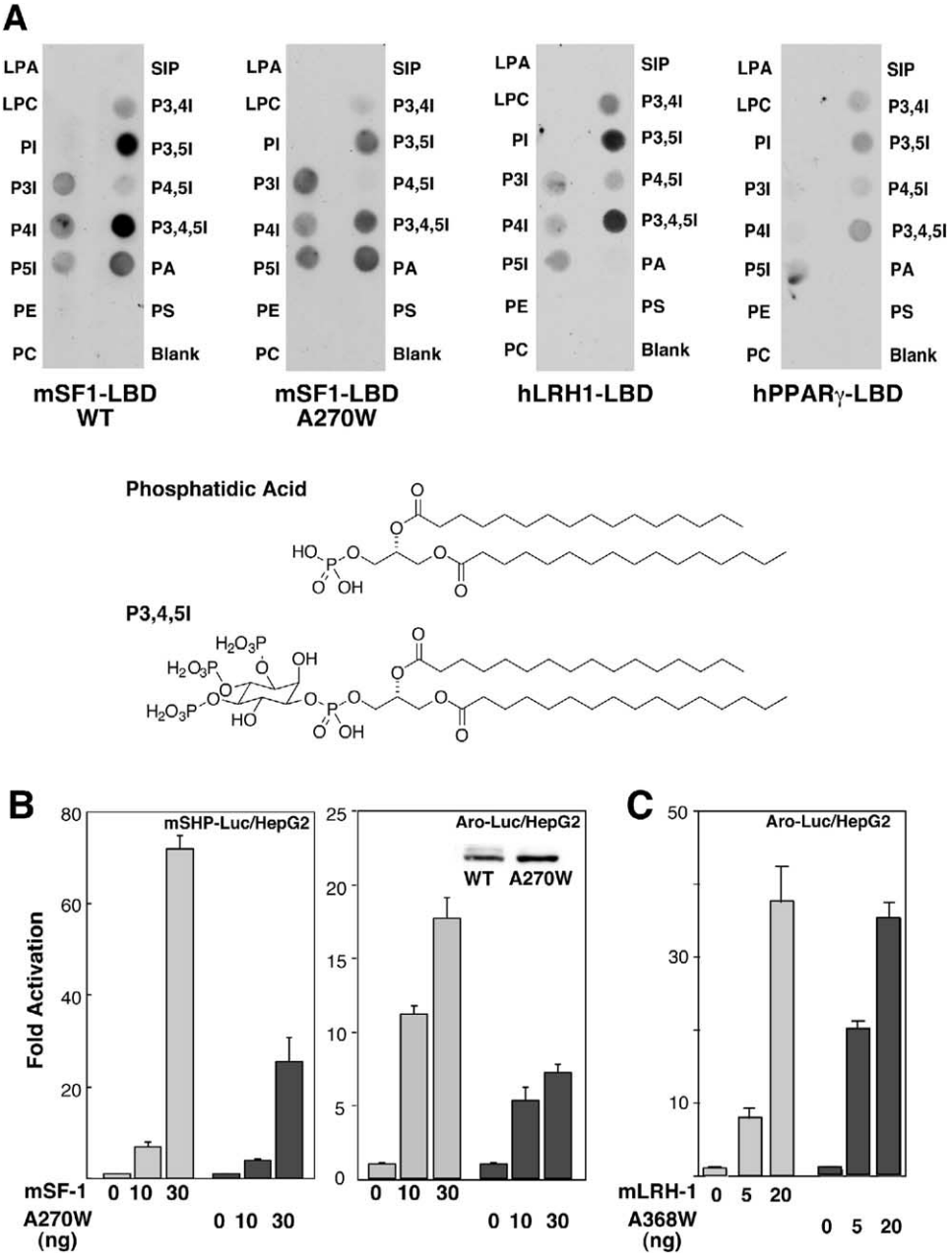

Figure 3. Selective Binding to Phosphorylated Phosphatidyl Inositols by mSF-1 and Loss of Activity with mSF-1 Pocket Mutant

(A) Binding patterns to immobilized phospholipids for mSF-1, the mSF-1 A270W pocket mutant, hLRH-1, and a control protein apo-hPPARγ are shown with the identity of each phospholipid indicated. Levels of all four proteins incubated were equivalent (data not shown). Quantification of binding by wild-type mutant mSF-1 LBD protein (A270W) showed selective binding to all PIP_2 and PIP_3 species by 1.85- to 3.1-fold. Abbreviations are as follows: lysophosphatidic acid (LPA), lysophosphocholine (LPC), sphingosine-1-phosphate (SIP), phosphatidic acid (PA), phosphatidyl choline (PC), serine (PS), ethanolamine (PE), phosphatidyl inositol (PI), phosphatidyl (3), (4), or (5) inositiol monophosphate (P3I), (P4I), or (P5I), phosphatidyl (3,4), (3,5), or (4,5) inositol bisphosphate (P3,4I), (P3,5I) (P4,5I), and finally phosphatidyl (3,4,5) inositol triphosphate (PIP_3). Chemical structures are shown for PA and P3,4,5I.

(B) Activities of pocket mutants made in comparable positions in helix H3 for mSF-1 (A270W mSF-1) are shown following transfections in HepG2 human cells with two luciferase reporters, the aromatase, and mouse SHP promoters. Relative luciferase activities are shown as fold activation for each receptor at increasing concentrations (ng per 24 well plate), as indicated on the X axis.

(C) The luciferase activity is shown for the corresponding helix H3 A368W pocket mutant for mLRH-1 on the aromatase promoter in HepG2 cells.

ligands appears critical for mSF-1 activity as evidenced by the diminished activity exhibited by A270W mSF-1 pocket mutant (Figure 3C, refer back to Figure 2B). This same mutation when made in mLRH-1 (A368W, H3) caused little or no loss of activity in cellular assays, as previously observed (Figure 3C and Sablin et al. [2003]).

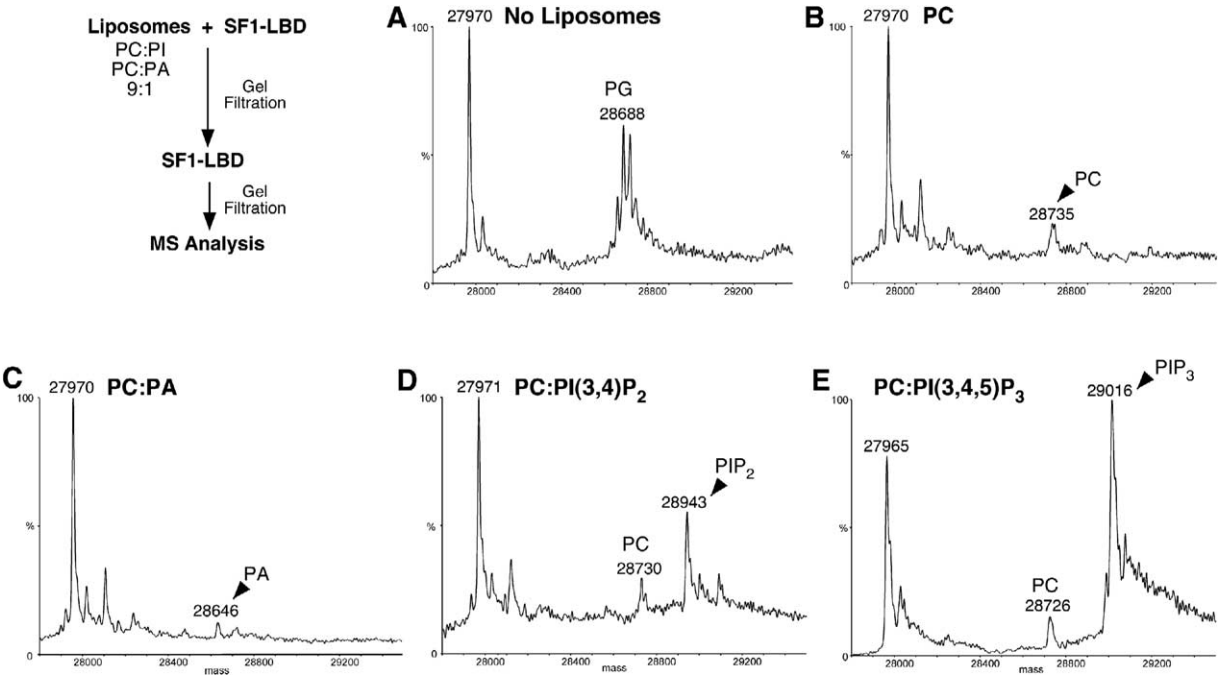

Figure 4. Selective Binding of Phosphatidyl Inositols to mSF-1

In the upper left corner, a flow diagram is shown for ligand analyses of mSF-1 LBD protein following incubation with different liposomes, as described in Experimental Procedures. Mass spectra profiles (ESI-LC/MS) are shown for the basal state (No Liposomes, panel A), and after incubations with the neutral liposomes of phosphatidyl choline (PC, panel B), with phosphatidic acid liposomes (PC:PA [9:1], panel C), and with phosphatidyl inositol liposomes PC:PI(3,4)P_2 [9:1] (PIP_2, panel D) or PC:PI(3,4,5)P_3 [9:1] (PIP_3, panel E). In (B), (D), and (E), the small peaks at mass 28730 Da are PC liganded receptor (PC), and in (C), the peak at mass 28646 is PA liganded receptor (PA). Direct mass spectrometry analysis (without gel filtration) on the PC:PA-receptor sample revealed a strong peak of free phosphatidic acid (data not shown), showing that ample PA was present in the PC:PA liposomes.

The binding of phospholipids was further explored by mass spectrometry analysis of purified LBD proteins after incubation with liposomes containing phosphatidyl choline (PC), mixed with either phosphatidic acid (PA), PI(3,4)P_2, or PI(3,4,5)P_3 in a 9:1 ratio. Remarkably, incubation of the mSF-1 LBD with the neutral PC liposome showed an almost complete loss of the bacterial PG phospholipid with very little exchange or binding by PC; similar results were found with the PC:PA liposome (Figures 4B and 4C) with both profiles differing greatly from spectra observed with the PG bound state of the mSF-1 LBD (Figure 4A, No Liposomes). In contrast, efficient binding was observed for PI(3,4)P_2 or PI(3,4,5)P_3 as evidenced by the increase mass of 970 and 1050 Da, respectively, with only a small uptake of PC observed (Figures 4D and 4E). A similar experiment carried out with mLRH-1 LBD revealed less selectivity compared to that of mSF-1, with equal exchange of PC, PI(3,4)P_2, or PI(3,4,5)P_3, as well as some liganded PA detected (see Supplemental Figure S2). These data taken together with the PIP strip binding data suggest that SF-1s and hLRH-1 bind much more robustly and selectively to phosphorylated PIs than does mLRH-1. The structural basis for this species difference in selective phospholipid binding is discussed below.

Regulation of NR5 Receptors Activity

NR5A receptors are coexpressed with and repressed by the orphan nuclear receptors, Dax-1 and SHP (Figure 5A). These orphan nuclear receptors contain a putative LBD but no DBD; their capacity to repress SF-1, LRH-1, and steroid hormone receptors is mediated by regions within the very N- and C-terminal LBD (Holter et al., 2002; Ito et al., 1997; Nachtigal et al., 1998). Unlike NR4 orphan receptors (Nurr1, DHR38) that have lost their coactivator cleft (Baker et al., 2003; Wang et al., 2003), all four LBD structures of SF-1 and LRH-1 exhibit a well-formed docking site for coregulators. Peptide binding assays were carried out for both mLRH-1 and mSF-1 LBD proteins using C-terminal fluorescently tagged SHP and Dax-1 peptides and fluorescence anisotropy, as described (Moore et al., 2004). Selective high-affinity binding was found for both mLRH-1 and mSF-1, with SF-1 binding more tightly to peptides from Dax-1; only the N-terminal LXXLL motif in the Dax-1 LBD region is able to bind both mSF-1 and mLRH-1 (Figures 5A and 5B).

As observed with NR/coactivator complexes, bound SHP-1 peptide in the coactivator cleft is positioned by hydrophobic contacts between the peptide leucines and LBD surface residues, and by hydrogen bonds between the backbone carbonyl and the conserved arginine (mArg282, hArg281), and the backbone amide with the conserved glutamate (mGlu455, hGlu454) found in helices H4 and H12, respectively (Figure 5C, left panel). Further, superposition of the mSF-1/SHP-1 structure with the apo-structure of mLRH-1 shows little change in the positions of helices H3, H4, and H12 contacting

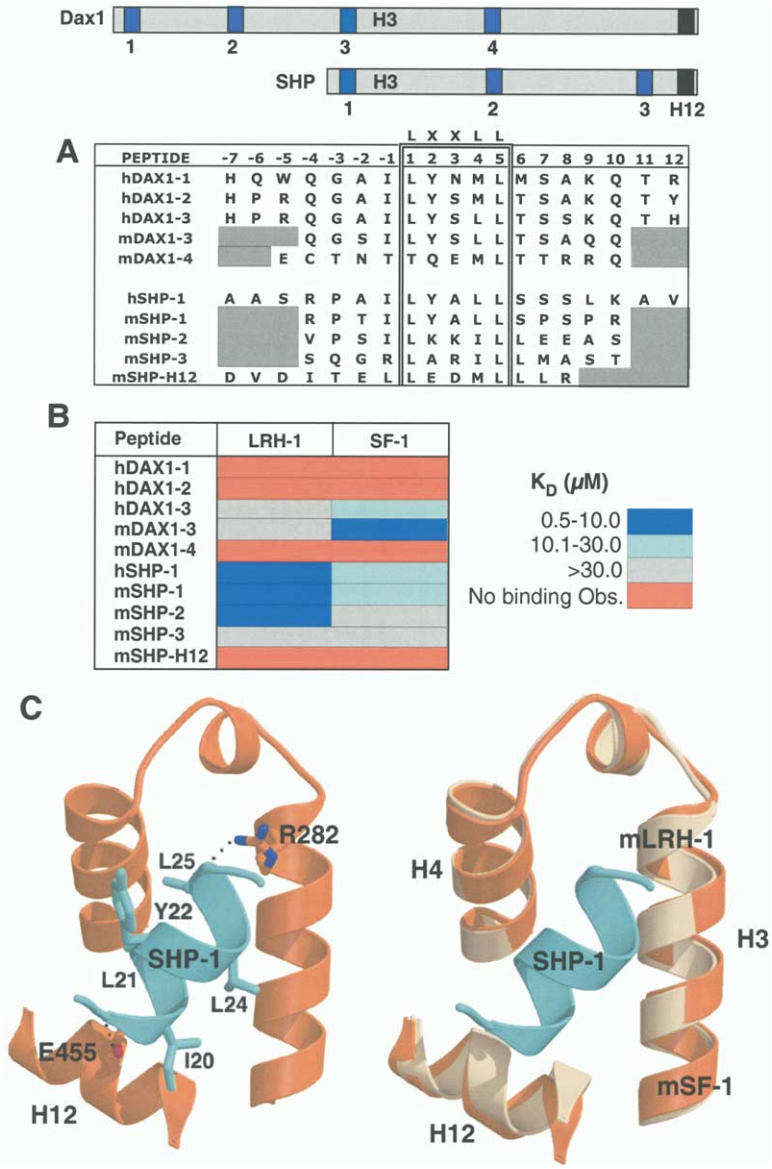

Figure 5. SHP and Dax-1 Binding to mSF-1 and mLRH-1

(A) Schematics of SHP and Dax-1 are shown with colored boxes corresponding to LXXLL peptides used in the fluorescence anisotropy assay, as depicted and listed in the table.

(B) Relative binding affinities for labeled peptides are indicated by color-coded affinities (K_d values) ranging from 0.5–10.0, 10.1–30.0, and >30.0 μM and were determined as described in Experimental Procedures. The mSHP-1 peptide used in crystallization of mSF-1 is RPTILYALLSPSPR (mSHP-1).

(C) Ribbon depiction of the mSHP-1 peptide in the coactivator cleft of mSF-1 (orange ribbon) or superposed with the mLRH-1 structure (beige ribbon). Residues are numbered according to the database entry Q62227 for mSHP.

the peptide (Figure 5C, right panel). Similarly, conformations of LBDs and ligands were found to be nearly identical when hSF-1 was crystallized with or without TIF-2 (Figures 1C and 2E). Taken together, these data suggest that selectivity of corepressor (Dax-1 and SHP) or coactivator binding to NR5A receptors is mediated by flanking amino acids. Moreover, NR5A receptors adopt a seemingly "active conformation" at all times, as opposed to classic ligand-dependent receptors (Darimont et al., 1998). Activity levels achieved by this class of receptor would then depend on ligand, post-translational modifications, and levels of coregulators. Thus, simply increasing corepressor levels, such as Dax-1, may override ligand-dependent activation and shift the receptor into an inactive state. This notion is partially supported by genetic data showing dosage of Dax-1 to be critical in mammalian sexual development, where SF-1 regulates multiple genes (reviewed in Ludbrook and Harley, 2004), and by the fact that SF-1 and LRH-1 regulate Dax-1 and SHP in a negative feedback regulatory mechanism (Lu et al., 2000).

Compared with LRH-1, SF-1 exhibits a shorter helix H2 and a more flexible region connecting helices H2 and H3 (Figure 6A). The mutation R314M, predicted to disrupt a 2.7 Å salt bridge between Arg314 (H5) and Glu238 (H2) in mSF-1 but not to interfere with ligand binding, sharply diminished receptor activity (Figure 6B), suggesting that the integrity of the NR5 receptors is mediated in part by packing interaction between helix H2 and other helices in the body of receptor. Interestingly, this same mutation when made in mLRH-1 (R412M) showed a much more modest decrease than observed with the analogous SF-1 R314M mutant—in mLRH-1 this interaction with corresponding shorter side chain of Asp236 is predicted to be less important, suggesting that additional interactions at the more extended H2-H3 interface in LRH-1 help to stabilize the receptor structure.

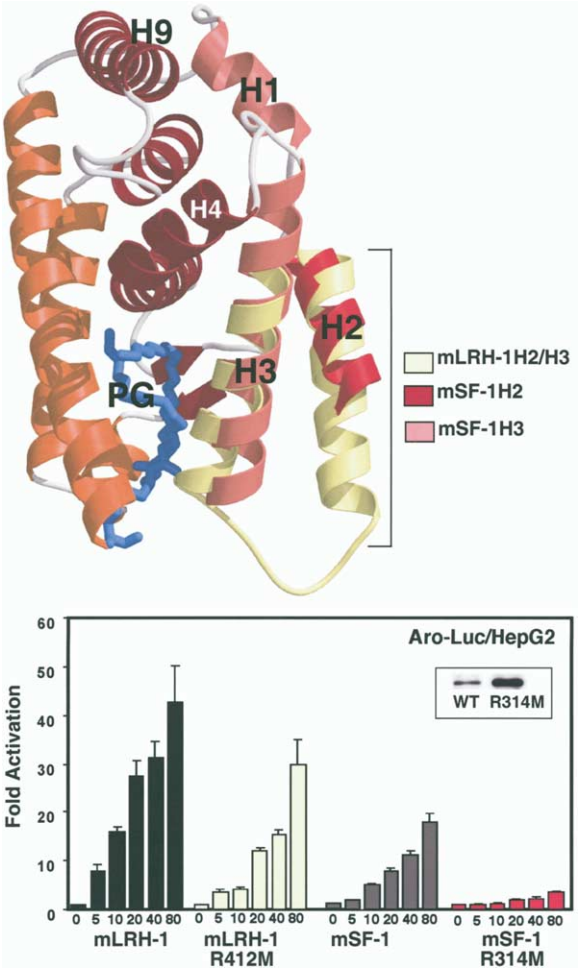

Figure 6. The Role of H2/H3 Structural Elements in Maintaining an Active Conformation of mLRH-1 and mSF-1

In the top panel, ribbon diagrams of partial structures of mLRH-1 and mSF-1 are shown. Helices H2 (red) and H3 (pink) of mSF-1 are superposed with the helices H2 and H3 of mLRH-1 (light yellow), and the phosphatidyl glycerol ligand is shown (blue stick). The H2 of mSF-1 is approximately half the length of helix H2 in mLRH-1 H2. The bottom panel shows reporter activity in HepG2 cells with increasing concentrations of wild-type and helix H5 mutants for both mLRH-1 and mSF-1. Relative luciferase activities are shown.

Species Difference in the Ligand Binding Pocket

The structures of NR5A receptors allow us to identify specific elements that facilitate phospholipid binding in the mouse and human SF-1s and human LRH-1 but diminish it in mouse LRH-1. For all receptors, only hydrophobic interactions are made between the 33 residues contacting the PG phospholipid; residues contacting the ligand are listed for all four LBDs (Supplemental Table S1). Direct comparison of these residues shows conserved changes between SF-1 and LRH-1, with most differences adding mass to unoccupied space in the mLRH-1 ligand-free pocket. However, when comparing species, a cluster of nonconserved residue changes that span helices H6-H7 is noted between human and mouse LRH-1 (Figure 7A); on the other hand, only one residue difference occurs between mouse and human SF-1. Further analysis shows residues within this cluster to be crucial for phospholipid binding. Indeed, binding of this ligand is optimized by coordination of the phosphate head group at the base of the pocket, with hydrogen bonding provided by Gly342 at the beginning of H6, and Tyr437 and Lys441 at the end of H11, which are 2.8 Å, 2.6 Å, and 2.8 Å from the ligand, respectively (Figure 7B). These interactions effectively seal the bottom of the ligand binding pocket with the phosphate group from the ligand contributing to this closure (Figure 7C).

A different scenario occurs in mLRH-1, where Glu440 forms a strong ionic interaction with the opposing Lys539 in helix H11 (analogous to Lys441 in mSF-1), sealing the pocket and stabilizing the mLRH-1 LBD in the absence of the ligand (Figure 7C). The other unique residues spanning helices H6-H7 in mLRH-1 (Thr439 and Phe443, Figure 7A) are also predicted to minimize ligand binding by clashing with both the phosphate group and aliphatic chains, respectively. To test the hypothesis that key residues interacting with the lipid's phosphate group are critical to ligand binding, mLRH-1 was "humanized" by an E440G mutation. Wild-type and mutant receptors were assayed before and after reducing cellular pools of phosphatidic acid and subsequent phosphatidyl inositols with a competitive inhibitor of phospholipase D (Fang et al., 2001). N-butanol treatment had a marginal effect on the activity of mLRH-1 but substantially reduced activation by the humanized E440G mLRH-1, and to a lesser extent wild-type mSF-1 (Figure 7D). Collectively, these data are consistent with the lowered selectively observed for mLRH-1 phospholipid binding and are predicted by structures of the LRH-1 and SF-1 orthologs.

Recent Divergence in the Rodent LRH-1

Evolutionary analysis of structure-function relations in the LRH-1/SF-1 subfamily indicates that ligand binding is the ancestral state for these proteins where ligand binding was subsequently reduced or altered in the lineage leading to the rodent LRH-1. We coded the presence or absence of ligand binding as a phylogenetic character and reconstructed its evolution on the phylogeny of the NR5A gene family (Figure 8). As described in Experimental Procedures, both maximum parsimony and maximum likelihoods were used to evaluate two hypotheses concerning the function of the common ancestor of the entire NR5A subfamily—that the ancestor was liganded (H_1) and that it was unliganded (H_0). Under H_1, a single loss of ligand binding is required on the branch leading to the rodent LRH-1, whereas H_0 requires ligand binding to have been gained independently in the SF-1 and human LRH-1 lineages. H_1 is therefore the most parsimonious hypothesis. A maximum likelihood analysis assuming that ligand binding can be gained or lost under a simple reversible Markov process also supports H_1, albeit nonsignificantly, indicating a loss of ligand binding in rodent LRH-1s (likelihood ratio = 3.05).

To increase the power of our analysis, we analyzed the evolution of the key sequence sites that have been structurally identified as critical for ligand binding in NR5A receptors. Although functional data from structures

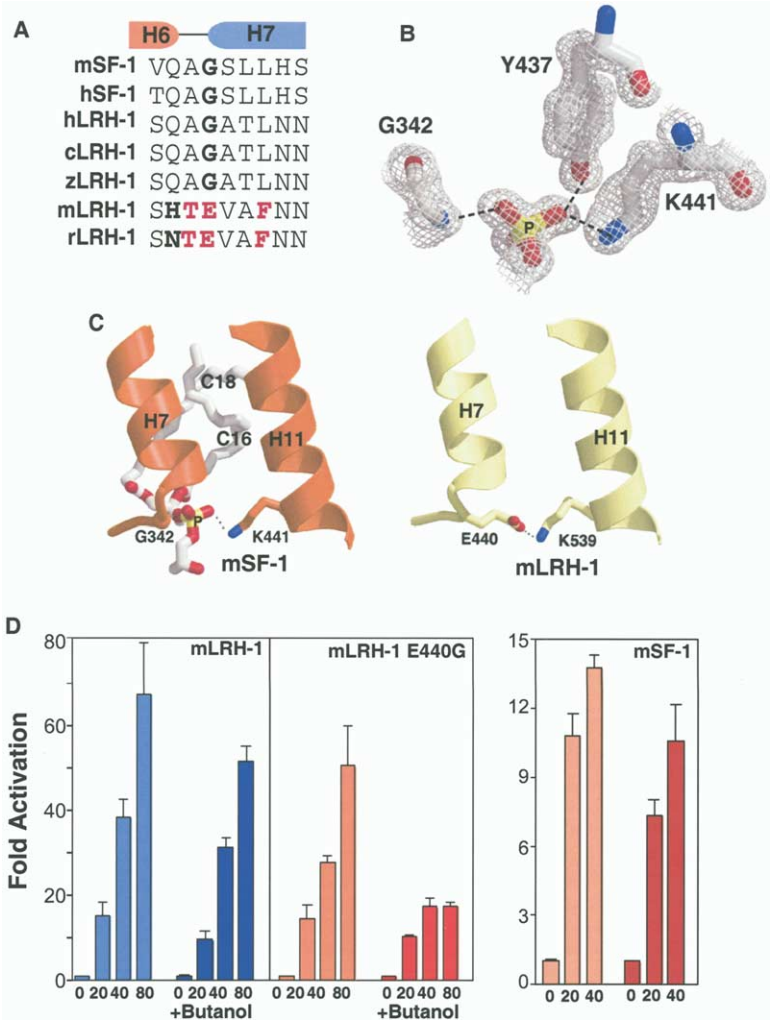

Figure 7. Species Differences in the Closure of the Ligand Binding Pocket

(A) Sequence alignment of the region spanning helices H6 and H7 is shown for a limited number of species. Rodent LRH-1-specific changes are highlighted in red.

(B) Electron density showing coordination of the phosphate group by three residues in mSF-1. These include Gly342 (H7) and Tyr437 and Lys441 (H11) with hydrogen bonds indicated (dashed line). The phosphate is labeled (P).

(C) Interactions between helices H7 and H11 are depicted for mSF-1, with phospholipid ligand (white stick) and for mLRH-1 without ligand. The salt bridge between Glu440 and Lys539 in mLRH-1 is depicted.

(D) Reporter activity is shown after depletion of phosphatidic acid by butanol with wild-type mLRH-1, mSF-1, and "humanized" mLRH-1 E440G mutant transfected into HepG2 cells. Activity is expressed as fold activation using the aromatase luciferase reporter.

are known for only four family members, sequences are available for dozens. We used maximum likelihood (Yang et al., 1995) to determine ancestral amino acid states and evolutionary changes in the H6-H7 residues corresponding to Thr439, Glu440, and Phe443 in rodent LRH-1 (TEF, Figure 8). These sites were chosen because, as discussed above, structural and experimental evidence indicates that they exclude or diminish phospholipid binding in mLRH-1, but the homologous residues, Ala, Gly, and Leu, confer ligand binding on hLRH-1 and the SF-1s (AGL, Figure 8). The NR5A ancestral sequence has all three ligand-associated states (AGL), and this reconstruction has extremely high confidence (posterior probability 100% for each site). The derived TEF residues that close the pocket in the absence of ligand all evolved much later on than the branch leading to the rodent LRH-1 (posterior probability 100% for each site). Examination of the genetic code indicates that each of these replacements can be conferred by a single base-pair mutation.

These findings strongly corroborate the hypothesis that ligand binding was ancestral in the SF-1/LRH-1 family and was later lost or radically diminished in rodent LRH-1s due to a small number of specific amino acid replacements. The lost or altered ligand binding state in rodent LRH-1 is the second example of a taxon-specific nuclear receptor losing the capacity to bind ligand from a liganded ancestor; the other is the estrogen receptor ortholog of the mollusc *Aplysia californica* (Thornton et al., 2003). These findings cast doubt on the hypothesis that ligand binding in the nuclear receptor superfamily was independently gained numerous times from an ancestral orphan receptor (Escriva et al., 2000). If the loss of ligand dependence is common and requires only a few sequence changes, the opposite scenario—repeated loss of ligand binding from a liganded ancestor—may better characterize NR evolution.

Finally, the finding that the rodent LRH-1 has diverged from other members of the family is of interest in light of differences noted in both bile acid and cholesterol transport for humans and mice (Dietschy and Turley, 2002). While species differences can be attributed to the absence of the murine cholesterol transport protein (CETP) (Lie et al., 2002), there are notable differences in the regulation of LRH-1 targets (Cyp7A1, Cyp8B, and SHP) involved in cholesterol homeostasis (Delerive et al., 2004; Fayard et al., 2004).

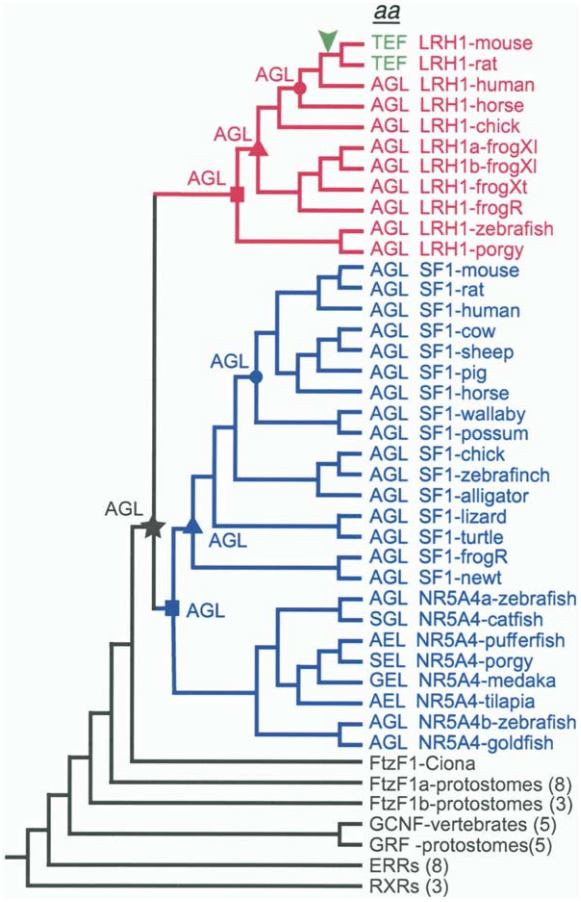

Figure 8. Amino Acids that Coordinate Ligand in SF-1 Are Ancestral

The maximum posterior probability phylogeny of the NR5 gene family is shown, including LRH-1s (red), SF-1s (blue), and outgroup sequences (black, with number of sequences analyzed shown in parentheses). Residues homologous to mLRH-1 positions 439, 440, and 443 are shown for each LRH-1/SF-1 sequence (aa). Maximum likelihood reconstructions of ancestral amino acid states are shown for SF-1 and LRH-1 proteins in the last common ancestor of vertebrates (squares), of tetrapods (triangles), and of mammals (circles), as well as for the common ancestral gene preceding the duplication that split the SF-1 and LRH-1 lineages (star). All ancestral reconstructions have 100% posterior probability. Green arrowhead shows acquisition of amino acids that exclude ligand in the rodent LRH-1 lineage and loss of ligand binding on the same branch. Species names and accession numbers are provided in Supplemental Table S2.

Do LRH-1/SF-1 Function as Nuclear Phospholipid Sensors?

That the bacterial phospholipid (PG) adopts an identical conformation, filling both hLRH-1 and SF-1 pockets equally well, offers a strong structural argument that this "fortuitous" ligand resembles closely the native ligand. Furthermore, phosphatidyl inositols shown here to bind NR5A receptors are predicted to adopt a similar conformation. Thus, our collective structural and biochemical data support phospholipids as ligands for both SF-1 and hLRH-1; this result is unexpected given the role that each plays in cholesterol transport or cholesterol metabolism in sterol synthesis. This proposal implies that a distinct pool of cellular lipids signal via modulation of the NR5A nuclear receptors. Indeed, the literature suggests that nuclear phosphatidyl inositol lipids exist as well as enzymes affecting their metabolism, such as phosphatidyl inositol 3-kinase (PI-3K) (Irvine, 2002; Ledeen and Wu, 2004; Martelli et al., 2003). Additionally, both PI-3 and PI-5 phosphatases exhibit prominent nuclear staining (Bacqueville et al., 2001; Deleris et al., 2003), thus providing a mechanism to downregulate PI nuclear signaling. Although we found that Wortmannin (PI-3 kinase inhibitor) and the PI-3 phosphatase PTEN affected the activities of wild-type and pocket mutant SF-1 receptors differently (I.N.K., unpublished data), further studies and additional pharmacological tools are needed to selectively disrupt nuclear phospholipid signaling pathways. Nonetheless, the link between PI-3 kinase signaling and NR5A receptor activity is intriguing given the roles that both SF-1 and LRH-1 play in cell proliferation. Indeed, haploinsufficiency of both *sf-1* and *lrh-1* leads to decreased cell proliferation (Bland et al., 2000; Botrugno et al., 2004), while increased gene dosage of *SF-1* is reported to be associated with human adrenal cortical tumors (de Figueiredo et al., 2004). Because PI-3 kinase pathways are known to regulate cell cycle progression and cell growth, it is tempting to speculate that extracellular events that trigger this pathway might also elevate nuclear PIs, and thus modulate SF-1/LRH-1 activities.

Finally, it is worth considering how phospholipids are delivered to nuclear receptors. Cytoplasmic shuttling of PIs to the plasma membrane is carried out by phosphatidyl inositol transport proteins (PITP) in an ATP-independent manner; these proteins are also present in the nucleus. Crystal structures of phospholipid binding proteins show a large hydrophobic pocket or tunnel able to bind lipids (Yoder et al., 2001; Hsuan and Cockcroft, 2001; Soccio and Breslow, 2003). Whether PIs are directly taken up by SF-1/LRH-1 from membranes (due to transient receptor shuttling between the cytoplasm and nucleus) or are delivered by nuclear phospholipid binding proteins remains unclear. While many questions are still to be answered, our current study leads us to hypothesize phosphatidyl inositols as bona fide ligands for NR5A receptors and, as such, provide a direct link between transcription and phospholipid signaling.

Experimental Procedures

Protein Purification and Crystallization

The mSF-1 LBD (219–462) was engineered by mutating cysteines at 302, 408, 413, and 423 to prevent oxidation (mSF-1 residue number follows accession NP_620639). Modified HIS6-tagged mSF-1 LBD was expressed and purified by Ni-Trap affinity purification followed by cleavage of HIS-tag with recombinant tobacco etch viral protease, as previously described for mLRH-1 LBD (Sablin et al., 2003). HIS6-tagged hSF-1 (222–461) and hLRH-1 (300–542) were expressed using the pRSETa vector, purified by Ni-NTA chromatography, followed by cleavage of the HIS6-tag using thrombin. Crystallization conditions for hSF-1 with and without the coactivator peptide TIF-2 are described in detail in Madauss et al. (2004), and crystals were obtained in 0.1 M TRIS (pH 7.8), 0.4 M $MgCl_2$, 13% PEG6000, 5 mM DTT. For mSF-1, equal volumes of mSF-1 LBD were added to a 6-fold molar excess of mSHP-1 peptide (RPTILYALLSPSPR) in 14% PEG8K, 0.1 M TRIS (pH 7.5), 5% isopropanol, and 15% xylitol to produce in 5 days large (200 μm) crystals that

diffracted to 1.1–1.2 Å. Data were integrated using DENZO and scaled with SCALEPACK. For hLRH-1, the protein and TIF-2 peptide were mixed in equal volumes with 1.2 M sodium potassium phosphate (pH 4.9), 4% (v/v) glycerol, 4% (v/v) ethylene glycol. Crystals were grown at 22°C and appeared in one week and reached 100–200 μm in each dimension over a period of 3 weeks. Prior to data collection, hLRH-1 crystals were dipped in cryoprotectant (reservoir solution containing 11.5% glycerol and 11.5% ethylene glycol) and flash-frozen in liquid nitrogen. The TIF-2 peptide sequence is KENALLRYLLDKDD and was used for both hLRH-1 and hSF-1 crystallization. X-ray data were collected at IMCA 17-ID line (Argonne, Illinois), and data were processed and scaled with HKL2000. The hLRH-1 model was built by molecular replacement with Amore program using hSF-1 as a search model and refined with CNS. In this model, a second TIF-2 peptide is found in the asymmetric unit and forms loose contacts with the tail of the first TIF-2 peptide positioned in the coactivator cleft formed by H3, H4, and H12 of the hLRH-1 receptor. Rebuilding between rounds of refinement was performed with the graphics program QUANTA.

Cell Culture and Transfections

Human HepG2 liver carcinoma cells were plated the day of transfection in 24 well plates and transfected with FUGENE 6 with amounts of DNA indicated in figures and legends. For all experiments, 200 ng/well of luciferase reporter were used and pCI-Neo-β-gal (50 ng/well) were transfected along with wild-type or mutant receptors. Luciferase activity was measured after 48 hr, as previously described (Sablin et al., 2003). Expression of all mutants was tested by Western blot analyses using anti-HA antibody (Covance) directed against an N-terminal tag. In all cases, mutant receptors were expressed at equivalent or higher levels than wild-type protein. For N-butanol experiments, 0.1% 1-butanol was added for 2 hr. All transfection experiments were done in triplicates and repeated at least three times; representative experiments are shown with standard errors indicated by bars.

Ligand Analyses and Phospholipid Binding Assays

Protein samples were desalted and injected onto a column packed with P6 gel (BioRad) to exchange nonvolatile buffers with 20 mM ammonium acetate (pH 6.8). Buffer-exchanged protein was collected and back flushed at a flow rate of 0.75–1 μl/min into a nanoflow electrospray ionization source fitted on a Waters/Micromass QTOF-1 (Beverly, Massachusetts) mass spectrometer. Data were collected in positive ion mode over a mass range of 1000–4000 m/z. For structural determination of ligands, a similar in-gel filtration apparatus was connected to an orthogonal acceleration time-of-flight mass spectrometer (LCMSD-TOF, Agilent) and a quadrupole ion trap mass spectrometer (LCMSD Trap SL, Agilent). Samples were examined utilizing negative ion electrospray using conditions that denatured the protein-ligand complex.

PIP Strips™ (Echelon) were first blotted for 1 hr with Casein hydrolysate (Sigma) dissolved in TBST buffer. HIS6-tagged LBD proteins were added at a concentration of 1.5 μM and incubated at 4°C overnight, followed by incubation at 25°C for 4 hr. Proteins were detected with rabbit polyclonal anti-His antibody (Immunology Consultants Laboratory). For liposome preparations, lipids (4 μM) were mixed in chloroform/methanol and dried under reduced pressure to form a lipid film. Lipids were as follows: 1-palmitoyl-2-oleoyl-sn-glycero-3-phosphate (PA) and 1-palmitoyl-2-oleoyl-sn-glycero-3-phosphocholine (PC) were from Avanti Polar Lipids (Alabaster, Alabama), and 1,2-dipalymitoyl-sn-glycero-3-phosphoinositol 3,4-bisphosphate ($PI(3,4)P_2$) and 1,2-dipalymitoyl-sn-glycero-3-phosphoinositol 3,4,5-trisphosphate ($PI(3,4,5)P_3$) were from Echelon Biosciences Inc (Salt Lake City, Utah). Liposomes were formed at pH 7.6 TRIS buffered saline by vortexing and immersed in a bath sonicator for 1–2 hr under argon at room temperature to facilitate formation of uniformly mixed small unilamellar vesicles. Particle zeta average size was determined using a Malvern (Southborough, Massachusetts) Zeta3000 Dynamic Light Scattering Instrument. Neutral liposomes were prepared with 100% PC and found to be 70.6 ± 0.4 nm. All other liposomes were prepared at a lipid ratio of PC:nonPC [9:1] and found to be 46.4 ± 1.4 nm for PC:PA, 37.1 ± 3.8 nm for PC:$PI(3,4)P_2$, and 31.2 ± 1.4 nm for PC:$PI(3,4,5)P_3$. Under these conditions, PI and PA lipids should mix completely into stable bilayers and consist primarily of PC. LBD proteins (2 mg/ml) were exchanged into liposome buffer and combined with the liposomes to produce a 25:1 molar ratio of PC to protein and a 2.5:1 molar ratio of PA, $PI(3,4)P_2$, or $PI(3,4,5)P_3$ to protein. Mixtures were incubated for 20 hr at room temperature, and protein was separated from liposomes by gel-filtration on Superdex 75 (Pharmacia), concentrated, subjected to another round of gel filtration, and analyzed by mass spectrometry as described above. The amount of SF-1 LBD protein associated with free liposomes (void volume) following gel filtration was determined to be <1% for all liposome species.

Peptide Binding Assays

LBD proteins were serially diluted from 150 μM to 0.002 μM in binding buffer (50 mM NaPO4, 150 mM NaCl, pH 7.2, 1 mM DTT, 1 mM EDTA, 0.01% NP40, 10% glycerol). Diluted protein was added to fluorescent coregulator peptide (20 nM) in 384 well plates yielding final protein concentrations of 75–0.001 μM and 10 nM of fluorescent peptide. Samples were analyzed as previously described (Moore et al., 2004). Construction of 20 aa coregulator peptides with the general motif of CXXXXXXXLXXL/AL/AXXXXXXX were as follows: peptides were synthesized in parallel using standard fluorenylmethoxycarbonyl (Fmoc) chemistry in 48 well synthesis blocks (FlexChem System, Robbins) (Wellings and Atherton, 1997). Coupling efficiency was monitored and the completed peptides were cleaved from the resin, followed by reversed-phase chromatography and mass spectrometry (MALDI-TOF/ESI) to purify the peptides, and are described in Moore et al. (2004).

Evolutionary Analysis

Protein sequences of 48 SF-1/LRH-1/FtzF1 family members with full-length ligand binding domains were obtained from GenBank by BLAST search using *Homo sapiens* SF-1 as a query. Twenty additional sequences from the closely related ERR, GCNF/GRF, and RXR groups (Thornton and DeSalle, 2000) were also obtained to serve as outgroup sequences. (See Supplemental Table S2 for accession numbers and species names). These sequences were aligned using ClustalX 1.83 software (Thompson et al., 1994) assuming a gap:change cost ratio of 10. The phylogeny of the gene family was then inferred from the aligned sequences using the Bayesian Markov Chain Monte Carlo method (Ronquist and Huelsenbeck, 2003) implemented in MrBayes v. 3.0 software. Tree and parameter space were explored with four simultaneous chains (three heated) for 300,000 generations each, using the Jones model of protein evolution with a four-category discrete γ model of among-site rate variation. Priors were equal for tree topologies, uniform (0,10) for branch lengths, and uniform (0.1, 5) for the α shape parameter of the γ distribution. The initial 100,000 trees, a point well past stationarity, were discarded as burn-in.

Phylogenetic reconstruction of the ancestral states at internal nodes for ligand binding or ligand independence, coded as a binary character, were conducted by parsimony and maximum likelihood. For the former, we used Fitch's parsimony algorithm (Fitch, 1971) on a simple tree consisting of the four taxa for which ligand binding states are known (Sablin et al., 2003; this paper). For maximum likelihood reconstruction, we calculated the likelihood of each ancestral state 0 (no ligand binding) and 1 (ligand binding) as the probability of evolving the terminal states in mLRH-1, hLRH-1, mSF-1, and hSF-1, given the phylogeny that relates these genes, and a simple reversible Markov process for transitions between states 0 and 1 (Pagel, 1999). The probability P_{ij} of observing a state change on a tree branch of length k is P_{ij} =

$$\frac{1}{2} - \frac{1}{2}e^{-k}.$$

Branch lengths were assumed equal a priori and scaled to their maximum likelihood values by hill climbing; unknown states at internal nodes other than the NR5A ancestor were treated as nuisance parameters and optimized by maximum likelihood.

Ancestral amino acid states for positions in the sequence alignment corresponding to 439, 440, and 443 in mLRH-1 were reconstructed using the marginal Bayesian maximum likelihood method of Yang (Yang et al., 1995), as implemented in PAML 3.14 software,

assuming a Jones model of amino acid evolution and a four-category γ model of rate variation among sites (α optimized by ML). The tree for ancestral state reconstruction was the maximum posterior probability tree from the Bayesian analysis, adjusted at three nodes that had posterior probability <0.95 to make them consistent with known taxonomic relationships among species (see Supplemental Figure S3). Branch lengths for the ancestral reconstruction were optimized by maximum likelihood using PAML software.

Supplemental Data

Supplemental Data include three figures and two tables and can be found with this article online at http://www.cell.com/cgi/content/full/120/3/343/DC1/.

Acknowledgments

We would like to thank Drs. D. Julius, K. Shokat, D. Stokoe, S. Wadekar, N. Jouravel, D. Moore, and F. Szoka for critical comments, experimental suggestions, and reagents. The IMCA-CAT beamline 17-ID (or 17-BM) at the Advanced Photon Source was supported by the companies of the Industrial Macromolecular Crystallography Association through a contract with Illinois Institute of Technology. We would like to thank Drs. Cheng Yang and Joseph Ferrara from Rigaku/MSC Inc. for an invitation to this facility. This work was funded by NIH 1R21-GM70792-1 and the Oregon Medical Research Foundation to J.W.T., a HHMI predoctoral fellowship to J.A.M., and a NIDDK-PO1 support to R.J.F., R.K.G., and H.A.I.

Received: November 3, 2004
Revised: January 13, 2005
Accepted: January 27, 2005
Published: February 10, 2005

References

Bacqueville, D., Deleris, P., Mendre, C., Pieraggi, M.T., Chap, H., Guillon, G., Perret, B., and Breton-Douillon, M. (2001). Characterization of a G protein-activated phosphoinositide 3-kinase in vascular smooth muscle cell nuclei. J. Biol. Chem. *276*, 22170–22176.

Baker, K.D., Shewchuk, L.M., Kozlova, T., Makishima, M., Hassell, A., Wisely, B., Caravella, J.A., Lambert, M.H., Reinking, J.L., Krause, H., et al. (2003). The Drosophila orphan nuclear receptor DHR38 mediates an atypical ecdysteroid signaling pathway. Cell *113*, 731–742.

Billas, I.M., Moulinier, L., Rochel, N., and Moras, D. (2001). Crystal structure of the ligand-binding domain of the ultraspiracle protein USP, the ortholog of retinoid X receptors in insects. J. Biol. Chem. *276*, 7465–7474.

Bland, M.L., Jamieson, C.A., Akana, S.F., Bornstein, S.R., Eisenhofer, G., Dallman, M.F., and Ingraham, H.A. (2000). Haploinsufficiency of steroidogenic factor-1 in mice disrupts adrenal development leading to an impaired stress response. Proc. Natl. Acad. Sci. USA *97*, 14488–14493.

Botrugno, O.A., Fayard, E., Annicotte, J.S., Haby, C., Brennan, T., Wendling, O., Tanaka, T., Kodama, T., Thomas, W., Auwerx, J., and Schoonjans, K. (2004). Synergy between LRH-1 and beta-catenin induces G1 cyclin-mediated cell proliferation. Mol. Cell *15*, 499–509.

Christenson, L.K., McAllister, J.M., Martin, K.O., Javitt, N.B., Osborne, T.F., and Strauss, J.F., 3rd. (1998). Oxysterol regulation of steroidogenic acute regulatory protein gene expression. Structural specificity and transcriptional and posttranscriptional actions. J. Biol. Chem. *273*, 30729–30735.

Darimont, B.D., Wagner, R.L., Apriletti, J.W., Stallcup, M.R., Kushner, P.J., Baxter, J.D., Fletterick, R.J., and Yamamoto, K.R. (1998). Structure and specificity of nuclear receptor-coactivator interactions. Genes Dev. *273*, 30729–30735.

de Figueiredo, B.C., Cavalli, L.R., Pianovski, M.A., Lalli, E., Sandrini, R., Ribeiro, R.C., Zambetti, G., Delacerda, L., Rodrigues, G.A., and Haddad, B.R. (2004). Amplification of the steroidogenic factor 1 (SF-1) gene in childhood adrenocortical tumors. J. Clin. Endocrinol. Metab. Published online November 2004. 10.1210/jc.2004-0942

Deleris, P., Bacqueville, D., Gayral, S., Carrez, L., Salles, J.P., Perret, B., and Breton-Douillon, M. (2003). SHIP-2 and PTEN are expressed and active in vascular smooth muscle cell nuclei, but only SHIP-2 is associated with nuclear speckles. J. Biol. Chem. *278*, 38884–38891.

Delerive, P., Galardi, C.M., Bisi, J.E., Nicodeme, E., and Goodwin, B. (2004). Identification of liver receptor homolog-1 as a novel regulator of apolipoprotein AI gene transcription. Mol. Endocrinol. *18*, 2378–2387.

Desclozeaux, M., Krylova, I.N., Horn, F., Fletterick, R.J., and Ingraham, H.A. (2002). Phosphorylation and intramolecular stabilization of the ligand binding domain in the nuclear receptor steroidogenic factor 1. Mol. Cell. Biol. *22*, 7193–7203.

Dhe-Paganon, S., Duda, K., Iwamoto, M., Chi, Y.I., and Shoelson, S.E. (2002). Crystal structure of the HNF4 alpha ligand binding domain in complex with endogenous fatty acid ligand. J. Biol. Chem. *277*, 37973–37976.

Dietschy, J.M., and Turley, S.D. (2002). Control of cholesterol turnover in the mouse. J. Biol. Chem. *277*, 3801–3804.

Escriva, H., Delaunay, F., and Laudet, V. (2000). Ligand binding and nuclear receptor evolution. Bioessays *22*, 717–727.

Fang, Y., Vilella-Bach, M., Bachmann, R., Flanigan, A., and Chen, J. (2001). Phosphatidic acid-mediated mitogenic activation of mTOR signaling. Science *294*, 1942–1945.

Fayard, E., Auwerx, J., and Schoonjans, K. (2004). LRH-1: an orphan nuclear receptor involved in development, metabolism and steroidogenesis. Trends Cell Biol. *14*, 250–260.

Fitch, W.M. (1971). Toward defining the course of evolution: minimal change for a specific tree topology. Syst. Zool. *20*, 406–416.

Holter, E., Kotaja, N., Makela, S., Strauss, L., Kietz, S., Janne, O.A., Gustafsson, J.A., Palvimo, J.J., and Treuter, E. (2002). Inhibition of androgen receptor (AR) function by the reproductive orphan nuclear receptor DAX-1. Mol. Endocrinol. *16*, 515–528.

Hsuan, J., and Cockcroft, S. (2001). The PITP family of phosphatidylinositol transfer proteins. Genome Biol. *2*, REVIEWS3011.

Ingraham, H.A., Lala, D.S., Ikeda, Y., Luo, X., Shen, W.H., Nachtigal, M.W., Abbud, R., Nilson, J.H., and Parker, K.L. (1994). The nuclear receptor steroidogenic factor 1 acts at multiple levels of the reproductive axis. Genes Dev. *8*, 2302–2312.

Irvine, R.F. (2002). Nuclear lipid signaling. Sci. STKE, http://stke.sciencemag.org/cgi/content/full/OC_sigtrans;2002/150/re13.

Ito, M., Yu, R., and Jameson, J.L. (1997). DAX-1 inhibits SF-1-mediated transactivation via a carboxy-terminal domain that is deleted in adrenal hypoplasia congenita. Mol. Cell. Biol. *17*, 1476–1483.

Kallen, J.A., Schlaeppi, J.M., Bitsch, F., Geisse, S., Geiser, M., Delhon, I., and Fournier, B. (2002). X-ray structure of the hRORalpha LBD at 1.63 A. Structural and functional data that cholesterol or a cholesterol derivative is the natural ligand of RORalpha. Structure (Camb.) *10*, 1697–1707.

Lala, D.S., Syka, P.M., Lazarchik, S.B., Mangelsdorf, D.J., Parker, K.L., and Heyman, R.A. (1997). Activation of the orphan nuclear receptor steroidogenic factor 1 by oxysterols. Proc. Natl. Acad. Sci. USA *94*, 4895–4900.

Ledeen, R.W., and Wu, G. (2004). Nuclear lipids: key signaling effectors in the nervous system and other tissues. J. Lipid Res. *45*, –.

Lee, M.K., Lebedeva, L., Suzawa, M., Wadekar, S., Desclozeaux, M., and Ingraham, H.A. (2005). Repression of orphan nuclear receptor activity via SUMO-modification and the Dead-Box Protein DP103 (Ddx20, Gemin-3). Mol. Biol. Cell *25*, 1879–1890.

Li, Y., Lambert, M.H., and Xu, H.E. (2003). Activation of nuclear receptors: a perspective from structural genomics. Structure (Camb.) *11*, 741–746.

Lie, J., de Crom, R., van Gent, T., van Haperen, R., Scheek, L., Lankhuizen, I., and van Tol, A. (2002). Elevation of plasma phospholipid transfer protein in transgenic mice increases VLDL secretion. J. Lipid Res. *43*, 1875–1880.

Lu, T.T., Makishima, M., Repa, J.J., Schoonjans, K., Kerr, T.A., Auwerx, J., and Mangelsdorf, D.J. (2000). Molecular basis for feedback regulation of bile acid synthesis by nuclear receptors. Mol. Cell *6*, 507–515.

Ludbrook, L.M., and Harley, V.R. (2004). Sex determination: a 'window' of DAX1 activity. Trends Endocrinol. Metab. *15*, 116–121.

Luo, X., Ikeda, Y., and Parker, K.L. (1994). A cell-specific nuclear receptor is essential for adrenal and gonadal development and sexual differentiation. Cell *77*, 481–490.

Madauss, K., Juzumiene, D., Waitt, G., Williams, J.P., and Williams, S.P. (2004). Generation and characterization of human steroidogenic factor 1 LBD crystals with and without bound co-factor peptide. Endocr. Res. *30*, 775–785.

Martelli, A.M., Tabellini, G., Borgatti, P., Bortul, R., Capitani, S., and Neri, L.M. (2003). Nuclear lipids: new functions for old molecules? J. Cell. Biochem. *88*, 455–461.

Mellon, S.H., and Bair, S.R. (1998). 25-Hydroxycholesterol is not a ligand for the orphan nuclear receptor steroidogenic factor-1 (SF-1). Endocrinology *139*, 3026–3029.

Moore, J.M., Galicia, S.J., McReynolds, A.C., Nguyen, N.H., Scanlan, T.S., and Guy, R.K. (2004). Quantitative proteomics of the thyroid hormone receptor-coregulator interactions. J. Biol. Chem. *279*, 27584–27590.

Nachtigal, M.W., Hirokawa, Y., Enyeart-VanHouten, D.L., Flanagan, J.N., Hammer, G.D., and Ingraham, H.A. (1998). Wilms' tumor 1 and Dax-1 modulate the orphan nuclear receptor SF-1 in sex-specific gene expression. Cell *93*, 445–454.

Pagel, M. (1999). Inferring the historical patterns of biological evolution. Nature *401*, 877–884.

Ronquist, F., and Huelsenbeck, J.P. (2003). MrBayes 3: Bayesian phylogenetic inference under mixed models. Bioinformatics *19*, 1572–1574.

Sablin, E.P., Krylova, I.N., Fletterick, R.J., and Ingraham, H.A. (2003). Structural basis for ligand-independent activation of the orphan nuclear receptor LRH-1. Mol. Cell *11*, 1575–1585.

Soccio, R.E., and Breslow, J.L. (2003). StAR-related lipid transfer (START) proteins: mediators of intracellular lipid metabolism. J. Biol. Chem. *278*, 22183–22186.

Steinmetz, A.C., Renaud, J.P., and Moras, D. (2001). Binding of ligands and activation of transcription by nuclear receptors. Annu. Rev. Biophys. Biomol. Struct. *30*, 329–359.

Thompson, J.D., Higgins, D.G., and Gibson, T.J. (1994). CLUSTALW: Improving the sensitivity of progressive multiple sequence alignment through sequence weighting, position-specific gap penalties and weight matrix choice. Nucleic Acids Res. *22*, 4673–4680.

Thornton, J.W., and DeSalle, R. (2000). A new method to localize and test the significance of incongruence: detecting domain shuffling in the nuclear receptor superfamily. Syst. Biol. *49*, 183–201.

Thornton, J.W., Need, E., and Crews, D. (2003). Resurrecting the ancestral steroid receptor: ancient origin of estrogen signaling. Science *301*, 1714–1717.

Wang, Z., Benoit, G., Liu, J., Prasad, S., Aarnisalo, P., Liu, X., Xu, H., Walker, N.P., and Perlmann, T. (2003). Structure and function of Nurr1 identifies a class of ligand-independent nuclear receptors. Nature *423*, 555–560.

Weatherman, R.V., Fletterick, R.J., and Scanlan, T.S. (1999). Nuclear-receptor ligands and ligand-binding domains. Annu. Rev. Biochem. *68*, 559–581.

Wellings, D.A., and Atherton, E. (1997). Standard Fmoc protocols. Methods Enzymol. *289*, 44–67.

Wisely, G.B., Miller, A.B., Davis, R.G., Thornquest, A.D., Jr., Johnson, R., Spitzer, T., Sefler, A., Shearer, B., Moore, J.T., Willson, T.M., and Williams, S.P. (2002). Hepatocyte nuclear factor 4 is a transcription factor that constitutively binds fatty acids. Structure (Camb.) *10*, 1225–1234.

Yang, Z., Kumar, S., and Nei, M. (1995). A new method of inference of ancestral nucleotide and amino acid sequences. Genetics *141*, 1641–1650.

Yoder, M.D., Thomas, L.M., Tremblay, J.M., Oliver, R.L., Yarbrough, L.R., and Helmkamp, G.M., Jr. (2001). Structure of a multifunctional protein. Mammalian phosphatidylinositol transfer protein complexed with phosphatidylcholine. J. Biol. Chem. *276*, 9246–9252.

Accession Numbers

Coordinates have been deposited in the Protein Data Bank as follows: mSF-1 PDB ID 1YMT, RCSB code RCSB031696, hLRH-1 PDB ID 1YOK and RCSB031753, and hSF-1 PDB ID 1YOW and RCSB031764.